A CRITICAL PLANE-BASED CRITERION FOR HIGH-CYCLE MULTIAXIAL FATIGUE USING AVERAGED PRINCIPAL STRESS DIRECTIONS

A. Carpinteri, A. Spagnoli, S. Vantadori

Department of Civil and Environmental Engng & Architecture, University of Parma, Parma (Italy)
E-mail: andrea.carpinteri@unipr.it; spagnoli@unipr.it; sabrina.vantadori@unipr.it

ABSTRACT

A high-cycle multiaxial fatigue criterion based on the so-called critical plane approach has recently been proposed by the present authors. Accordingly, the critical plane orientation is correlated to some averaged directions of the principal stresses, whereas other criteria available in the literature determine this orientation by maximizing the amplitude and/or the maximum value of some stress components. Then, fatigue strength estimation is performed by considering a quadratic combinations of the shear stress amplitude and the maximum value of the normal stress acting on the critical plane. The application of the proposed criterion for evaluating the endurance limit requires the knowledge of three material parameters: the fatigue limit under fully reversed normal stress, the fatigue limit under fully reversed shear stress, the slope of the S-N curve in the high-cycle regime for fully reversed normal stress. The purpose of the present paper is to critically highlight the main characteristics of the criterion.

1. INTRODUCTION

Several criteria have been proposed in the literature to assess the fatigue strength of structural components submitted to multiaxial loading in the high-cycle fatigue (HCF) regime. Generally speaking, the aim of these fatigue criteria is to reduce a given multiaxial stress/strain state to an equivalently effective uniaxial stress/strain condition. According to a number of comparative studies (for instance, see Refs [1,2]), the existing multiaxial fatigue criteria for HCF regime can be categorised according to the approach followed, namely: empirical formulae (Lanza, Manson, Haigh [1], Gough and Pollard [3], etc.), criteria based on the stress invariants, energy-based criteria, mesoscopic scale approach, etc.

Some criteria are based on the so-called critical plane approach, according to which the fatigue strength assessment is performed either in a plane where the amplitude or the maximum value of some stress components or a combination of them attains its maximum [4-9], or in plane whose orientation is correlated with that of some averaged principal stress directions [10-12].

In the present paper, a critical plane-based multiaxial HCF criterion recently proposed by the authors is reviewed and compared with some experimental data related to different brittle (hard) metals under non-proportional loading. The critical plane is determined by using averaged principal stress directions. Emphasis is herein placed on the main steps to be followed when applying the above criterion.

2. BASIC FRAMEWORK

According to the proposed criterion, the fatigue strength estimation in HCF (either endurance limit or total life estimation) is performed by analysing the time-varying stress tensor in a given point of the material submitted to multiaxial loading, under the assumption that the microcrack initiation stage is the critical one. Therefore, the criterion seems to be suitable for smooth or blunt notched structural components (e.g. see the recent work of Ref. [13] to characterise blunt notch geometry), where a very high fraction of the fatigue life is consumed during the microcrack initiation stage. As will be shown in the following, the criterion can successfully be applied to hard metals under any periodic proportional or non-proportional multiaxial loading. The main steps of the criterion are as follows [10-12,14]:

(i) Averaged directions of the principal stresses are determined on the basis of their instantaneous directions (two material parameters are required at this step: the fatigue limit σ_{af} under fully reversed normal stress, and the corresponding slope m of the S-N curve in the high-cycle regime);

(ii) The orientation of the initial (hereafter termed *critical*) crack plane and that of the final fracture plane are linked to the averaged directions of the principal stress axes (one further material parameter is required at this step: the fatigue limit τ_{af} under fully reversed shear stress);

(iii) The maximum value and the amplitude (in a loading cycle) of normal stress and shear stress, respectively, acting on the critical plane are determined;

(iv) The fatigue strength estimation is performed via a quadratic combination of normal and shear stress components acting on the critical plane (in the case of fatigue life estimation, one further material parameter might be required at this step: the slope m^* of the S-N curve in the high-cycle regime under fully reversed shear stress).

3. PRINCIPAL DIRECTIONS

3.1. Instantaneous directions of the principal stress axes

At a given material point P, the direction cosines of the instantaneous principal stress directions 1, 2 and 3 (being $\sigma_1(t) \geq \sigma_2(t) \geq \sigma_3(t)$) with respect to a fixed PXYZ frame can be worked out from the time-varying stress tensor $\boldsymbol{\sigma}(t)$. The orthogonal coordinate system P123 with origin at point P and axes coincident with the principal directions (Fig.1) can be defined through the "principal Euler angles", ϕ, θ, ψ, which represent three counter-clockwise sequential rotations around the Z-axis, Y'-axis and 3-axis, respectively ($0 \leq \phi < 2\pi$; $0 \leq \theta \leq \pi$; $0 \leq \psi < 2\pi$). The procedure to obtain the principal Euler angles from the direction cosines of the principal stress directions consists of two stages described in Ref. [9], and is rather lengthy, although very simple. The ranges of such Euler angles at the end of this two-stage procedure are reduced as follows : $0 \leq \phi,\ \theta \leq \pi/2$ and $-\pi/2 < \psi \leq \pi/2$.

As is well known, the instantaneous directions of the principal stresses do not vary with time in the case of a proportional loading (i.e. the loading case characterised by a time-varying stress tensor which can formally be written as $\boldsymbol{\sigma}(t) = f(t)\boldsymbol{\sigma}$, where $f(t)$ is a scalar time function and $\boldsymbol{\sigma}$ is a time-constant tensor of the stresses), whereas the opposite occurs for non-proportional loading. However, it is worth noticing that, also in the case of a proportional loading, principal stress directions might vary with respect to time as a result of principal stress ordering $\sigma_1 \geq \sigma_2 \geq \sigma_3$. This occurs, for instance, even in the simple case of uniaxial tension-compression (see Fig.2).

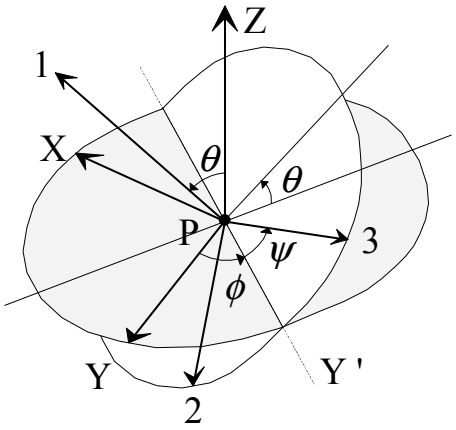

Figure 1: *Principal stress directions 1, 2, 3 described through the Euler angles* ϕ, θ, ψ

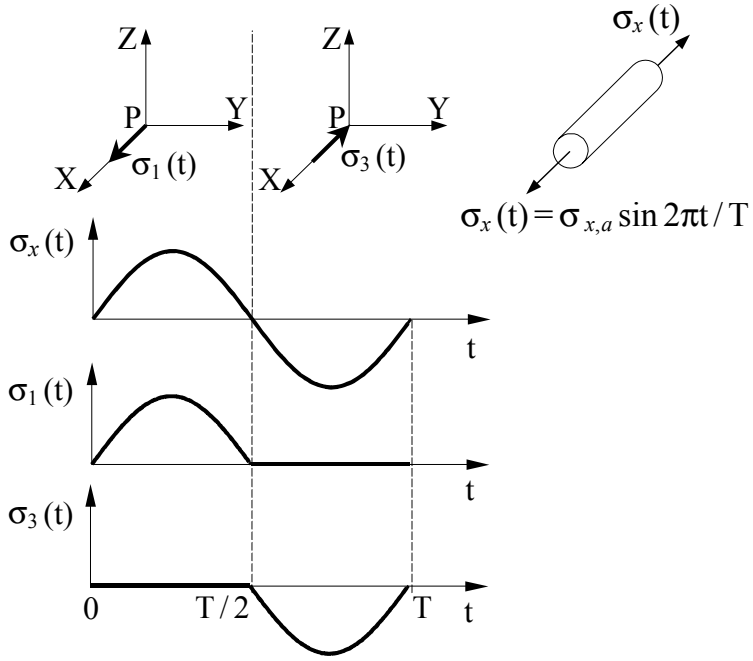

Figure 2: *Courses of principal stresses and changes of principal stress directions under sinusoidal tension–compression* $\sigma_x(t)$

3.2. Averaged directions of the principal stress axes

The averaged directions of the principal stress axes $\hat{1}, \hat{2}$ and $\hat{3}$ are obtained from the averaged values $\hat{\phi}, \hat{\theta}, \hat{\psi}$ of the principal Euler angles. Such values are computed by independently averaging the instantaneous values $\phi(t), \theta(t), \psi(t)$, as follows [15, 16]:

$$\hat{\phi} = \frac{1}{W}\int_0^T \phi(t) W(t)\, dt \qquad \hat{\theta} = \frac{1}{W}\int_0^T \theta(t) W(t)\, dt \tag{1}$$

$$\hat{\psi} = \frac{1}{W}\int_0^T \psi(t) W(t)\, dt \qquad W = \int_0^T W(t)\, dt$$

where T is the period of the cyclic load. The weight function $W(t)$ is given by:

$$W(t) = H\left[\sigma_1(t) - \frac{1}{2}\sigma_{af}\right]\left(\frac{\sigma_1(t)}{\sigma_{af}}\right)^{m_\sigma} \tag{2}$$

where $m_\sigma = -1/m$ and $H[\ ]$ is the Heaviside function ($H[x] = 1$ for $x > 0$, $H[x] = 0$ for $x \leq 0$). The proposed weight function is such that it includes into the averaging procedure those positions of the principal directions for which the maximum principal stress σ_1 is greater than half of the normal stress fatigue limit σ_{af} under fully reversed loading (a discussion for the adopted fraction of σ_{af} is presented elsewhere [10]).

4. CRITICAL PLANE AND FINAL FATIGUE FRACTURE PLANE

As has been pointed out by Brown and Miller [5], fatigue crack propagation can be distinguished into two stages: a first one in which a crack nucleates (near the external surface of a structural component) along a shear slip plane (*Stage 1*, *fatigue crack initiation plane*), and a second one in which crack propagation occurs in a plane normal to the direction of the maximum principal stress (*Stage 2*, *final fatigue fracture plane*). Thus, Stage 1 is characterised by a Mode II loading, whereas Stage 2 by a Mode I loading [7,17-19].

According to the criterion proposed by the present authors, the normal to the estimated final fatigue fracture plane of Stage 2, which is the one observed *post mortem* at the macro level, is assumed to be coincident with the averaged direction $\hat{1}$ of the maximum principal stress σ_1 [20] (such an assumption has been assessed to be realistic by comparing theoretical and experimental results [12]); this implies that the orientation of the final fatigue fracture plane depends not only on the time-varying stress state but also on the material parameters σ_{af} and m_σ . On the other hand, the *critical plane* is the verification material plane on which fatigue strength assessment is to be performed. Note that the orientation of the critical plane does not generally coincide with that of the final fatigue fracture plane (see below).

The orientation of the critical plane has been proposed to be correlated with the averaged directions of the principal stress axes [14]. In more detail, the empirical expression for δ (δ is the angle between the normal **w** to the critical plane and the averaged direction $\hat{1}$ of the maximum principal stress σ_1, where **w** belongs to the principal plane $\hat{1}\hat{3}$ as is shown in Fig. 3) is given by:

$$\delta = \frac{3\pi}{8}\left[1 - \left(\frac{\tau_{af}}{\sigma_{af}}\right)^2\right] \tag{3}$$

Equation 3 is valid for hard metals which are characterised by values of the ratio τ_{af}/σ_{af} ranging from $1/\sqrt{3}$ to 1 (note that the lower limit of τ_{af}/σ_{af} corresponds to the Von Mises strength criterion of mild metals for static loading). In the light of the above, the orientation of the critical plane depends on the time-varying stress state as well as the material parameters σ_{af}, τ_{af} and m_σ.

When the ratio τ_{af}/σ_{af} tends to $1/\sqrt{3}$ (threshold between mild and hard metals) the off angle δ tends to $\pi/4$. In this case, the critical plane tends to coincide with the actual fatigue crack initiation plane (Stage 1) for such materials. This is justified by the fact that, in the

HCF regime, the microcrack initiation stage is the critical one for the considered smooth or blunt notched structural components (made of mild-hard metals). On the other hand, when the ratio τ_{af} / σ_{af} tends to 1 (threshold between hard and extremely hard metals), the off angle δ tends to zero. This is in line with the fact that such materials have predominantly Stage 2 crack growth and, hence, the critical plane is assumed to coincide with the final fatigue fracture plane.

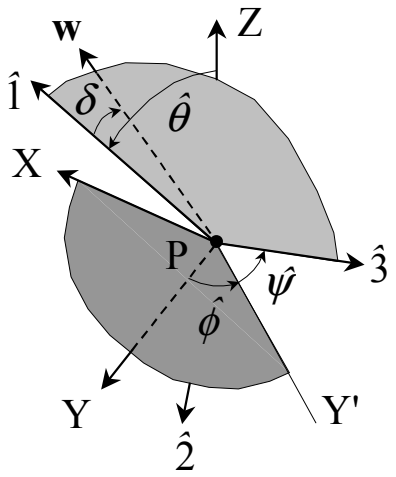

Figure 3: *Correlation between averaged principal stress directions* $\hat{1}\hat{2}\hat{3}$ *and normal* **w** *to the critical plane*

A value of δ equal to $\pi/4$ might be conjectured for $\tau_{af} / \sigma_{af} < 1 / \sqrt{3}$ (mild metals), whereas we can assume δ as equal to zero for $\tau_{af} / \sigma_{af} > 1$ (extremely hard metals). Some interesting observations on the variation of δ as a function of τ_{af} / σ_{af} can be found in Ref.[21].

5. FATIGUE STRENGTH ESTIMATION

5.1. Stress components acting on the critical plane

The critical plane Δ, passing through a given point P in the material, and the attached orthogonal coordinate system P*uvw* are considered (Fig.4), where the *w*-axis is normal to the critical plane. The direction cosines of *u*-, *v*- and *w*-axis can be computed, with respect to the PXYZ frame, as a function of the two angles φ and ϑ [14].

The stress vector $\mathbf{S_w}$ acting at a point P on the critical plane Δ can be expressed as follows:

$$\mathbf{S_w} = \boldsymbol{\sigma} \cdot \mathbf{w} \tag{4}$$

Then, the normal stress vector **N** and the shear stress vector **C** lying on the critical plane are:

$$\mathbf{N} = \left(\mathbf{w} \cdot \mathbf{S_w}\right) \mathbf{w} \tag{5}$$

$$\mathbf{C} = \mathbf{S_w} - \mathbf{N} \tag{6}$$

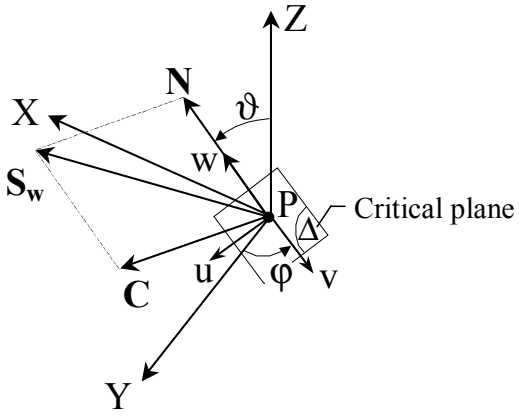

Figure 4: *Puvw and PXYZ coordinate systems (u- and v-axes belong to the critical plane Δ)*

For multiaxial constant amplitude cyclic loading, the vectors **N** and **C** are periodic functions of time. The direction of the normal stress **N**(t) is fixed with respect to time: consequently, the mean value N_m and the amplitude N_a of the normal stress can readily be calculated. On the other hand, the definitions of the shear stress mean value C_m and amplitude C_a are not unique, owing to the generally time-varying direction of **C**. The procedure proposed by Papadopoulos [22] has been adopted in Ref. [14] to determine the mean value C_m and the amplitude C_a of the shear stress vector **C**:

$$\begin{aligned} C_m &= \min_{\mathbf{C}'} \left\{ \max_{0 \le t \le T} \left\| \mathbf{C}(t) - \mathbf{C}' \right\| \right\} \\ C_a &= \max_{0 \le t \le T} \left\| \mathbf{C}(t) - C_m \right\| \end{aligned} \tag{7}$$

where the symbol $\|\cdot\|$ indicates the norm of a vector, $\mathbf{C}(t)$ is the shear vector at the time instant t, $\mathbf{C}'$ is a vector chosen according to the procedure presented in Ref. [22]. Note that, for proportional loading, we have $\boldsymbol{\sigma}(t) = f(t)\boldsymbol{\sigma}$ and, hence, $\mathbf{S_w}(t) = \boldsymbol{\sigma}(t) \cdot \mathbf{w} = f(t)\boldsymbol{\sigma} \cdot \mathbf{w}$ (see Eq. 4). Therefore, the direction of $\mathbf{S_w}$ and that of **C** (see Eq. 6) are fixed with respect to time, since $f(t)$ is a scalar time function.

5.2. Endurance limit

As a multiaxial fatigue limit condition, the following nonlinear combination of the maximum normal stress ($N_{\max} = N_m + N_a$) and the shear stress amplitude (C_a) acting on the critical plane has been proposed [14]:

$$\left(\frac{N_{\max}}{\sigma_{af}} \right)^2 + \left(\frac{C_a}{\tau_{af}} \right)^2 = 1 \tag{8}$$

Such a criterion is to some extent reminiscent of the well-known Gough ellipse [3]. However, conversely to the Gough's criterion, the proposed criterion considers stress components acting on the critical plane and, hence, it is capable of implicitly accounting for loading non-proportionality (e.g. the critical plane orientation depends on the phase angles between the stress components). In addition, some well-established experimental findings are included in

Eq. 8, namely: the mean shear stress C_m does not affect the HCF strength of hard metals [3], and the effect of the mean normal stress N_m is included.
In order to transform the actual constant amplitude periodic multiaxial stress state into an equivalent uniaxial normal stress amplitude $\sigma_{eq,a}$, Eq. 8 can be written as follows:

$$\sigma_{eq,a} = \sqrt{N_{\max}^2 + \left(\frac{\sigma_{af}}{\tau_{af}}\right)^2 C_a^2} = \sigma_{af} \tag{9}$$

5.3. Finite life fatigue strength

Using Basquin-like relationships for both fully reversed normal stress [$\sigma_a = \sigma_{af}\left(N_f / N_0\right)^m$; σ_a = amplitude of normal stress at fatigue life N_f; N_0 = reference number of cycles, e.g. $2 \cdot 10^6$] and fully reversed shear stress [$\tau_a = \tau_{af}\left(N_f / N_0\right)^{m^*}$; τ_a = amplitude of shear stress at fatigue life N_f], the number N_f of cycles to failure can be obtained from the solution of the following expression:

$$\sqrt{N_{\max}^2 + \left(\frac{\sigma_{af}}{\tau_{af}}\right)^2 \left(\frac{N_f}{N_0}\right)^{2m} \left(\frac{N_0}{N_f}\right)^{2m^*} C_a^2} = \sigma_{af}\left(\frac{N_f}{N_0}\right)^m \tag{10}$$

If the slope of the S-N curve for normal stress and that for shear stress coincide ($m = m^*$), the number N_f for a given multiaxial periodic stress state can explicitly be worked out from Eq.10:

$$N_f = N_0 \, \sigma_{af}^{m\sigma} \left[N_{\max}^2 + \left(\frac{\sigma_{af}}{\tau_{af}}\right)^2 C_a^2 \right]^{-\frac{m_\sigma}{2}} \tag{11}$$

6. SINUSOIDAL PLANE STRESS STATE

Let us consider the following biaxial normal stresses (σ_x, σ_y) and shear stress (τ_{xy}) at a given point P in the material, subjected to synchronous out-of-phase sinusoidal loading:

$$\begin{aligned} \sigma_x &= \sigma_{x,a} \, sin(2\pi \, t/T - \alpha) + \sigma_{x,m} \\ \sigma_y &= \sigma_{y,a} \, sin(2\pi \, t/T) + \sigma_{y,m} \\ \tau_{xy} &= \tau_{xy,a} \, sin(2\pi \, t/T - \beta) + \tau_{xy,m} \end{aligned} \tag{12}$$

where α is the phase angle between the stresses σ_x and σ_y, β is the phase angle between the stresses σ_y and τ_{xy}, the subscripts *a* and *m* stand for amplitude and mean value, respectively.

6.1. Instantaneous and averaged directions of the principal stress axes

As is well-known, the two non-zero principal stresses s_I and s_{II} in the stress plane XY are equal to:

$$s_{I,II} = \frac{\sigma_x + \sigma_y}{2} \pm \sqrt{\left(\frac{\sigma_x - \sigma_y}{2}\right)^2 + \tau_{xy}^2} \tag{13}$$

whereas the angle γ ($0° \leq \gamma \leq \pi/4$), which defines the absolute value of the inclination of the I-II principal stress directions with respect to the XY coordinate system, is given by:

$$\gamma = \frac{1}{2} arctg\left| 2\tau_{xy} / \left(\sigma_x - \sigma_y\right)\right| \tag{14}$$

The following cases may occur (see Fig. 1):

(a) $s_I, s_{II} > 0 \Rightarrow \sigma_1 = s_I,\ \sigma_2 = s_{II},\ \sigma_3 = 0$ (1-axis ≡ I-axis, 2-axis ≡ II-axis and 3-axis ≡ Z-axis);

(b) $s_I, s_{II} < 0 \Rightarrow \sigma_1 = 0,\ \sigma_2 = s_I,\ \sigma_3 = s_{II}$ (1-axis ≡ Z-axis, 2-axis ≡ I-axis and 3-axis ≡ II-axis);

(c) $s_I \geq 0, s_{II} \leq 0 \Rightarrow \sigma_1 = s_I,\ \sigma_2 = 0,\ \sigma_3 = s_{II}$ (1-axis ≡ I-axis, 2-axis ≡ Z-axis and 3-axis ≡ II-axis).

From the time-varying stress tensor, the courses of the principal Euler angles $\phi(t), \theta(t)$ and $\psi(t)$ can be determined. The specific values that the principal Euler angles can attain for the above cases (a) to (c) are as follows:

(a1) $\sigma_3 = 0;\quad \sigma_x \geq \sigma_y \Rightarrow \phi = \gamma;\quad \theta = \pi/2;\quad \psi = \pi/2$

(a2) $\sigma_3 = 0;\quad \sigma_x < \sigma_y \Rightarrow \phi = \pi/2 - \gamma;\quad \theta = \pi/2;\quad \psi = \pi/2$

(b1) $\sigma_1 = 0;\quad \sigma_x \geq \sigma_y \Rightarrow \phi + \psi = \gamma;\quad \theta = 0$

(b2) $\sigma_1 = 0;\quad \sigma_x < \sigma_y \Rightarrow \phi + \psi = \pi/2 - \gamma;\quad \theta = 0$

(c1) $\sigma_2 = 0;\quad \sigma_x \geq \sigma_y \Rightarrow \phi = \gamma;\quad \theta = \pi/2;\quad \psi = 0$

(c2) $\sigma_2 = 0;\quad \sigma_x < \sigma_y \Rightarrow \phi = \pi/2 - \gamma;\quad \theta = \pi/2;\quad \psi = 0$

As an example, a fully reversed normal stress σ_y with $\pi/2$ out-of-phase fully reversed shear stress τ_{xy} is considered (Fig. 5a). The biaxiality ratio $\lambda = \tau_{xy,a} / \sigma_{y,a}$ is assumed to be equal to 0.5 (in this case, the material plane experiencing the maximum amplitude of the shear stress, e.g. see McDiarmid criterion [7], is indeterminate), and the dimensionless applied normal stress amplitude $\tilde{\sigma}_{y,a} = 2\sigma_{y,a} / \sigma_{af}$ is assumed to be equal to 0.5. The courses of the principal stresses and the principal Euler angles are shown in Figs 5b and 5c, respectively. The resulting values of the averaged principal Euler angles are (m_σ is taken as equal to 10): $\hat{\phi} = 1.10,\ \hat{\theta} = \pi/2,\ \hat{\psi} = 0$. In particular, the angle η (with $\eta = \pi/2 - \hat{\phi}$) between the averaged direction $\hat{1}$ of the maximum principal stress σ_1 and the loading axis Y of the applied normal stress σ_y (e.g. Y coincides with the longitudinal axis of a specimen submitted to bending loading) results to be equal to 0.47 (i.e. about 27°). Figure 6 shows the variation of the angle η (expressed in degrees) as a function of the phase angle β, the biaxiality ratio λ, the dimensionless applied normal stress amplitude $\tilde{\sigma}_{y,a}$.

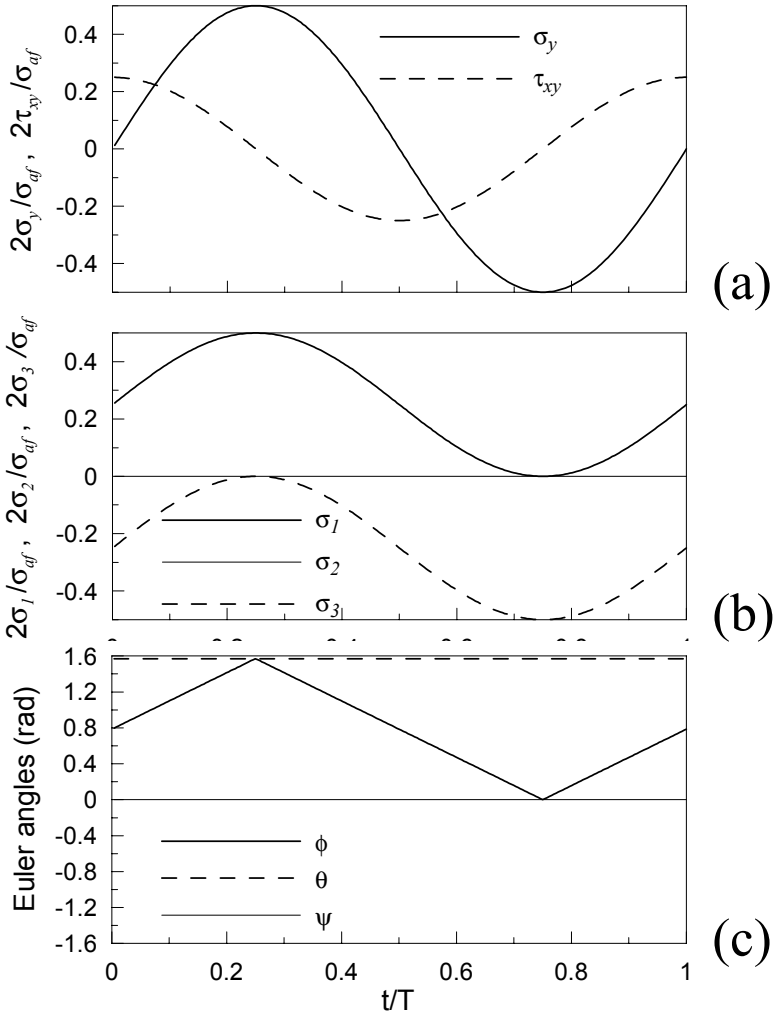

Figure 5: *Periodic time history of applied stresses (a), principal stresses (b) and principal Euler angles (c)*

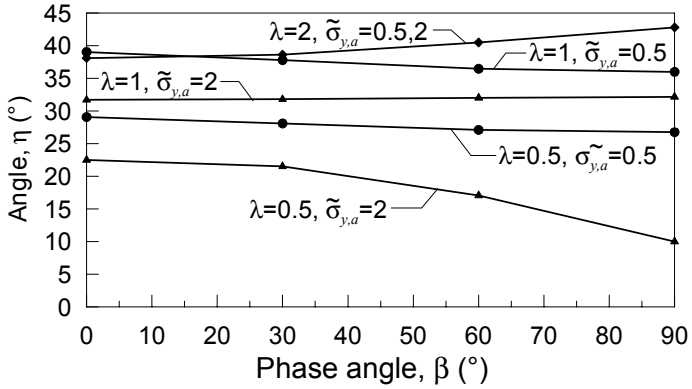

Figure 6: *The angle η (between the normal to the final fatigue fracture plane and the loading axis Y) against the phase angle β, for different values of the biaxiality ratio λ and the dimensionless applied normal stress amplitude $\tilde{\sigma}_{y,a}$ ($\eta = 0°$ for $\lambda = 0$ and $\eta = 45°$ for $\lambda = \infty$)*

6.2. Stress components acting on the critical plane

The stress vector $\mathbf{S_w}$, acting at a given point P on the critical plane Δ, can be computed as follows ($w \equiv (sin\vartheta cos\varphi; sin\vartheta sin\varphi; cos\vartheta)$, see Fig. 4) [14]:

$$\mathbf{S_w} = \boldsymbol{\sigma} \cdot \mathbf{w} \;\Rightarrow\; [S_w] = \begin{bmatrix} sin\vartheta\ (\sigma_x\, cos\varphi + \tau_{xy}\, sin\varphi) \\ sin\vartheta\ (\sigma_y\, sin\varphi + \tau_{xy}\, cos\varphi) \\ 0 \end{bmatrix} \tag{15}$$

The mean value N_m and the amplitude N_a of **N** can be determined by substituting the stress components (Eq. 12) into Eq. 5:

$$N_m = sin^2\vartheta\ [\sigma_{x,m} cos^2\varphi + \sigma_{y,m}\, sin^2\varphi + \tau_{xy,m}\, sin2\varphi] \tag{16}$$

and

$$N_a = \sqrt{a^2 + b^2}\ , \text{with} \tag{17a}$$

$$a = sin^2\vartheta\ [\sigma_{x,a}\ cos\alpha\ cos^2\varphi + \sigma_{y,a}\, sin^2\varphi + \tau_{xy,a} cos\beta\, sin2\varphi] \tag{17b}$$

$$b = -sin^2\vartheta\ [\sigma_{x,a}\, sin\alpha\, cos^2\varphi + \tau_{xy,a}\, sin\beta\, sin2\varphi] \tag{17c}$$

The shear stress vector **C** lying on the plane Δ is computed through Eq. 6:

$$\mathbf{C} = \begin{bmatrix} sin\vartheta\ [cos\varphi\ (\sigma_x cos^2\vartheta + (\sigma_x - \sigma_y)\, sin^2\vartheta\, sin^2\varphi) + \tau_{xy}\, sin\varphi\ (1 - 2\, sin^2\vartheta\, cos^2\varphi)] \\ sin\vartheta\ [sin\varphi\ (\sigma_y cos^2\vartheta + (\sigma_y - \sigma_x)\, sin^2\vartheta\, cos^2\varphi) + \tau_{xy}\, cos\varphi\ (1 - 2\, sin^2\vartheta\, sin^2\varphi)] \\ -sin^2\vartheta\ cos\vartheta\ (\sigma_x cos^2\varphi + \sigma_y\, sin^2\varphi + \tau_{xy}\, sin2\varphi) \end{bmatrix} \tag{18}$$

The values C_u and C_v of the components of **C** along the u- and v-axis are given by ($u \equiv (cos\vartheta cos\varphi; cos\vartheta sin\varphi; -sin\vartheta)$ and $v \equiv (-sin\varphi; cos\varphi; 0)$, see Fig. 4):

$$C_u = \mathbf{u} \cdot \mathbf{C} = f\, sin(\omega t) + g\, cos(\omega t) + C_{u,m} \tag{19a}$$

$$C_v = \mathbf{v} \cdot \mathbf{C} = p\, sin(\omega t) + q\, cos(\omega t) + C_{v,m} \tag{19b}$$

where the functions *f*, *g*, *p* and *q* are expressed by:

$$f = \frac{1}{2}\, sin2\vartheta\ [\sigma_{x,a} cos\alpha\, cos^2\varphi + \sigma_{y,a}\, sin^2\varphi + \tau_{xy,a} cos\beta\, sin2\varphi] \tag{20a}$$

$$g = -\frac{1}{2}\, sin2\vartheta\ [\sigma_{x,a}\, sin\alpha\, cos^2\varphi + \tau_{xy,a}\, sin\beta\, sin2\varphi] \tag{20b}$$

$$p = sin\vartheta\ \left[\frac{1}{2}\ (\sigma_{y,a} - \sigma_{x,a} cos\alpha)\, sin2\varphi + \tau_{xy,a} cos\beta\, cos2\varphi\right] \tag{20c}$$

$$q = -sin\vartheta\ \left[-\frac{1}{2}\, \sigma_{x,a}\, sin\alpha\, sin2\varphi + \tau_{xy,a}\, sin\beta\, cos2\varphi\right] \tag{20d}$$

and the mean values, $C_{u,m}$ and $C_{v,m}$, of the components C_u and C_v are given by:

$$C_{u,m} = \frac{1}{2}\, sin2\vartheta\ [\sigma_{x,m} cos^2\varphi + \sigma_{y,m}\, sin^2\varphi + \tau_{xy,m}\, sin2\varphi] \tag{21a}$$

$$C_{v,m} = sin\vartheta\ \left[\frac{1}{2}(\sigma_{y,m} - \sigma_{x,m})\, sin2\varphi + \tau_{xy,m}\, cos2\varphi\right] \tag{21b}$$

Equations 19 are the parametric equations of the ellipse **s** (Fig. 7) described by the tip of the shear stress vector **C** on the critical plane Δ during a loading cycle. This ellipse is centred at point ($C_{u,m}$; $C_{v,m}$), and its semi-axes can be computed as follows:

$$C_{a,b} = \sqrt{\frac{f^2+g^2+p^2+q^2}{2} \pm \sqrt{\left(\frac{f^2+g^2+p^2+q^2}{2}\right)^2 - (fq-gp)^2}} \tag{22}$$

Note that the amplitude of **C** coincides with the major semi-axis C_a of the above ellipse.

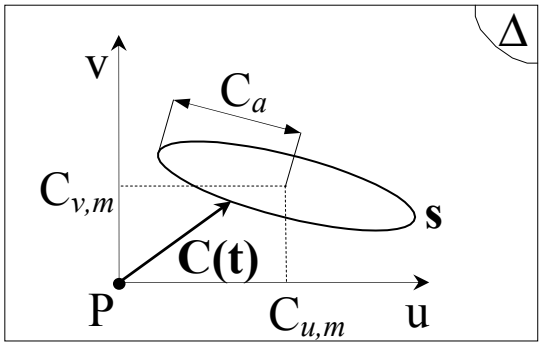

Figure 7: *Elliptic path* ***s*** *described by the tip of the shear stress vector* **C** *acting on the critical plane* Δ*, during a cycle of a synchronous out-of-phase sinusoidal plane stress state*

6.3. Comparison with experiments

An extensive comparison between the predictions of the present criterion, experimental results as well as predictions of other criteria has been carried out. The comparison has been performed for constant amplitude loading in terms of endurance limit and final fatigue fracture plane orientation [12,14,23] as well as, using an extended version of the criterion, for variable amplitude loading (random loading) in terms of fatigue life and final fatigue fracture plane orientation [24]. In the following, we briefly review some comparisons with experimental data related to synchronous in-phase or out-of-phase constant amplitude sinusoidal loading. In particular, the following fatigue tests on smooth specimens are analysed:

(i) bending and torsion (σ_y, τ_{xy}) [25];

(ii) bending and torsion with mean stress (σ_y, τ_{xy}) [26,27];

(iii) axial loading and internal pressure (σ_x, σ_y) [28].

The relevant material properties related to such experimental tests are reported in Table 1, whereas a summary of the loading conditions is reported elsewhere [14,23]. It needs here to be underlined that all loading cases being examined correspond to the multiaxial endurance limit state.

Table 1: *Material properties related to the experimental tests in Refs [25-28]*

		Materials	σ_{af} [MPa]	τ_{af} [MPa]	τ_{af}/σ_{af}	m_σ	*No. of test data*
(a)	Nishihara et al. [25]	Hard steel	313.9	196.2	0.63	8.7	12
(b)	Nishihara et al. [25]	Mild steel	235.4	137.3	0.58	18.2	10
(c)	Nishihara et al. [25]	Cast iron	96.1	91.2	0.95	19.4	8
(d)	Froustey et al. [26]	34Cr4	410.0	256.0	0.62	20.9	12
(e)	Zenner et al. [27]	30NCD16	660.0	410.0	0.62	13.2	10
(f)	Rotvel [28]	Low-carbon steel	215.8	127.2	0.59	14.5	6

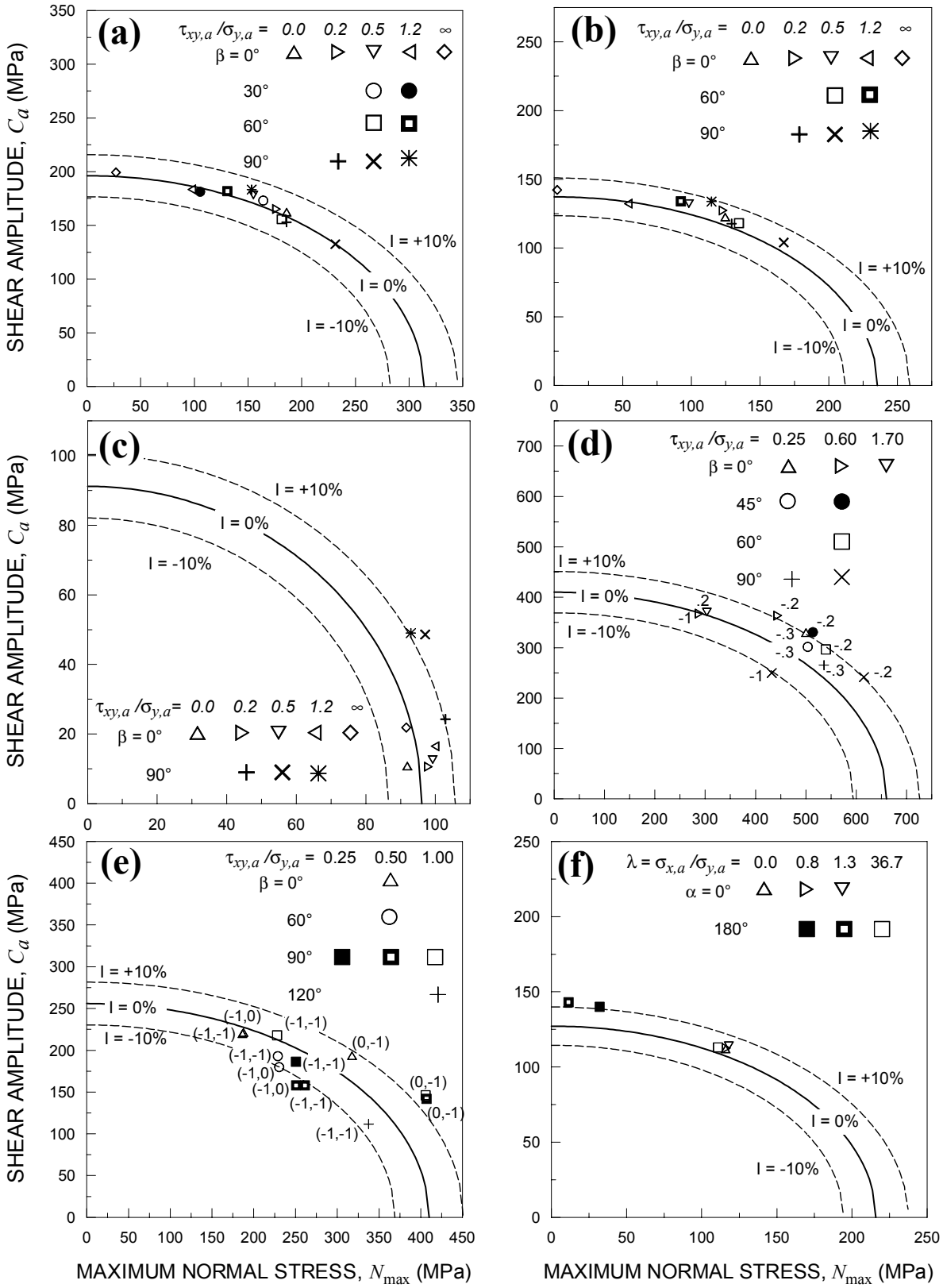

Figure 8: *Shear stress amplitude against maximum normal stress acting on the critical plane: theoretical predictions and experimental results [25-28]. For cases (a), (b), (c), (f), the loading ratios are equal to -1. For case (d), numbers near symbols refer to the loading ratio of σ_y (the loading ratio of τ_{xy} is equal to -1). For case (e), couples of numbers in brackets refer to the loading ratios of σ_y and τ_{xy}, respectively.*

By plotting the shear stress amplitude C_a against the maximum normal stress $N_{\max}$ acting on the critical plane, endurance limit state is exceeded when the experimental point with coordinates ($N_{\max}, C_a$) falls out of the ellipse with semi-axes equal to σ_{af} and τ_{af} (see Eq. 8). For the different materials and loading conditions being here considered, Figure 8 shows the correlation between this theoretical ellipse (continuous line) and the test results related to the endurance limit state. A good agreement exists since most of the experimental points fall very close to such an ellipse, between two dashed curves representing an error of ±10%.

7. CONCLUDING REMARKS

A high-cycle fatigue criterion based on the so-called critical plane approach for multiaxial periodic loading has been reviewed. The averaged principal stress directions determined through a weight function method are used to predict the orientation of the critical plane, understood as the plane on which fatigue strength estimation ought to be performed. Multiaxial endurance limit state is assessed using a nonlinear combination of the maximum value of the normal stress and the amplitude of the shear stress acting on the critical plane. The application of the criterion for endurance limit evaluation requires the knowledge of three material parameters (the fatigue limit under fully reversed normal stress, the fatigue limit under fully reversed shear stress, the slope of the S-N curve in the high-cycle regime for fully reversed normal stress), whereas one further material parameter (the slope of the S-N curve in the high cycle regime for fully reversed shear stress) is required for fatigue life calculation.

References

[1] Garud Y.S. (1981) Multiaxial fatigue: a survey of the state of the art. J. Testing Eval. **40**, 165-178.

[2] You B.-R., Lee S.-B. (1996) A critical review on multiaxial fatigue assessments of metals. Int. J. Fatigue **18**, 235-244.

[3] Gough H.J., Pollard H.V., Clenshaw W.J. (1951) Some experiments on the resistance of metals to fatigue under combined stresses. Aeronautical Res. Council Reports, R and M 2522, HMSO, London.

[4] Findley W.N. (1959) A theory for the effect of mean stress on fatigue of metals under combined torsion and axial load or bending. J. Engng Industry, Trans. ASME **81**, 301-306.

[5] Brown M.W., Miller K.J. (1973) A theory for fatigue failure under multiaxial stress-strain condition. Proc. Institute Mech. Engineers **187**, 745-755.

[6] Matake T. (1977) An explanation on fatigue limit under combined stress. Bull. JSME **20**, 257-263.

[7] McDiarmid D.L. (1991) A general criterion for high cycle multiaxial fatigue failure. Fatigue Fract. Engng Mater. Struct. **14**, 429-453.

[8] Susmel L., Lazzarin P. (2002) A bi-parametric Wöhler curve for high cycle multiaxial fatigue assessment. Fatigue Fract. Engng Mater. Struct. **25**, 63-78.

[9] Lazzarin P., Susmel L. (2003) A stress-based method to predict lifetime under multiaxial fatigue loading. Fract. Engng Mater. Struct. **26**, 1171-1187.

[10] Carpinteri A., Brighenti R., Macha E., Spagnoli A. (1999) Expected principal stress directions for multiaxial random loading-part I: theoretical aspects of the weight function method. Int. J. Fatigue **21**, 83-88.

[11] Carpinteri A., Brighenti R., Macha E., Spagnoli A. (1999) Expected principal stress directions for multiaxial random loading - Part II: Numerical simulation and experimental assessment through the weight function method. Int. J. Fatigue **21**, 89-96.

[12] Carpinteri A., Brighenti R., Spagnoli A. (2000) A fracture plane approach in multiaxial high-cycle fatigue of metals. Fatigue Fract. Engng Mater. Struct. **23**, 355-364.

[13] Atzori B., Lazzarin P., Meneghetti G. (2003) Fracture mechanics and notch sensitivity. Fatigue Fract. Engng Mater. Struct. **26**, 257-267.

[14] Carpinteri A., Spagnoli A. (2001) Multiaxial high-cycle fatigue criterion for hard metals. Int. J. Fatigue **23**, 135-145.
[15] Achtelik H., Macha E., Jakubowska I. (1983) Actual and estimated directions of fatigue fracture plane in Zl250 grey cast iron under combined alternating bending and torsion. Studia Geotechnica et Mechanica **5**, 2-30.
[16] Carpinteri A., Macha E., Brighenti R., Bryce R., Spagnoli A. (1997) Expected principal stress directions under multiaxial random loading through weight function method. In: Proc. 5th Int. Conf. Biaxial/Multiaxial Fatigue Fract., Cracow (Poland), 541-555.
[17] Brown M. W., Miller K. J. (1979) Initiation and growth of cracks in biaxial fatigue. Fatigue Fract. Engng Mater. Struct. **1**, 231-246.
[18] Socie D. (1987) Multiaxial fatigue assessment. In: Low-Cycle Fatigue and Elasto-Plastic Behaviour of Materials (Ed. Rie K.T.) Elsevier Applied Science, UK, 465-472.
[19] Macha E. (1989) Simulation investigations of the position of fatigue fracture plane in materials with biaxial loads. Mat.-Wiss.U. Werkstofftech. **20**, 132-136 and 153-163.
[20] Carpinteri A., Macha E., Brighenti R, Spagnoli A. (1999) Critical fracture plane under multiaxial random loading by means of Euler angles averaging. In: Multiaxial fatigue and fracture (Eds Macha E., Bedkowski W., Lagoda T), Elsevier Science Ltd, UK, 166-178.
[21] Liu Y., Mahadevan S. (2005) Multiaxial high-cycle fatigue criterion and life prediction for metals. Int. J. Fatigue **27**, 790-800.
[22] Papadopoulos I.V. (1998) Critical plane approaches in high-cycle fatigue: on the definition of the amplitude and mean value of the shear stress acting on the critical plane. Fract. Engng Mater. Struct. **21**, 269-285.
[23] Spagnoli A. (2001) A new high-cycle fatigue criterion applied to out-of-phase biaxial stress state. Int. J. of Mechanical Science **43**, 2581-2595.
[24] Carpinteri A., Spagnoli A., Vantadori S. (2003) A multiaxial fatigue criterion for random loading. Fatigue Fract. Engng Mater. Struct. **26**, 515-522.
[25] Nishihara T., Kawamoto M. (1945) The strength of metals under combined alternating bending and torsion with phase difference. Memories of the College Engng, Kyoto Imperial University **11**, 85–112.
[26] Froustey C., Lasserre S. (1989) Multiaxial fatigue endurance of 30NCD16 steel. Int. J. Fatigue **11**, 169-175.
[27] Zenner H., Heidenreich R., Richter I.Z. (1985) Fatigue strength under nonsynchronous multiaxial stresses. Mat. wiss u Werkstofftech **16**, 101–112.
[28] Rotvel F. (1970) Biaxial fatigue tests with zero mean stresses using tubular specimens. Int. J. Mech. Scie. **12**, 597–613.